OBSERVING THE ANGLE OF ATTACK OF THE TIP-PATH PLANE FROM ROTOR BLADE MEASUREMENTS

Lorenzo Trainelli, Carlo E.D. Riboldi, Mattia Bucari

Department of Aerospace Science and Technology, Politecnico di Milano, Milano, Italy

Abstract

A recurring problem in helicopters is the difficulty to accurately measure the angle of attack of the airframe and tip-path plane with respect to the slipstream. Differently from fixed wing aircraft, it is hard to find a spot on the airframe of a helicopter where the velocity vector of the stream is not polluted by a very relevant downwash component due to the deflecting action of the main rotor on the air stream. Furthermore, the geometrical definition of the tip-path plane calls for the knowledge of the attitude of the blades with respect to a plane normal to the main rotor mast. This attitude is related to the flap motion of the blades, which to this time cannot be measured effectively through a direct measurement method. Building on the experience and research results of the MANOEUVRES project, which is aimed at developing a novel sensor for the flap motion of the blades, making possible monitoring the noise intensity emitted by the helicopter during approach maneuvers, this paper presents a possible way to estimate the angle of attack of the tip-path plane starting from a basic set of measurements including those related to the flapping angle of the blades. The knowledge of the flap motion of the blades allows to observe also other flight mechanics performance parameters, like the thrust force coefficient, without the need for further sensor information. Support for the feasibility of the proposed observer comes from the well known equations for the flapping blade. The presented results assessing the quality of the synthesized observer and its ability to work under both design and off-design conditions have been obtained working on the virtual model of an existing machine.

1. INTRODUCTION

The problem of the estimation of the angle of attack of the tip-path plane (TPP) and other flight mechanics performance indexes has been fueled especially by the need to easily predict the noise footprint of the helicopter on the ground.

The problem of helicopter noise reduction has already received much attention in the past, as witnessed by the number of works devoted to the matter. Due to the complexity of the aerodynamic interactions giving birth to helicopter noise, and the consequent difficulties in the real time prediction of noise emission from on-board sensors,[1–4] preliminary research efforts have suggested solutions able to reduce noise mainly by means of a suitable design of the rotor blades.[5–8] Such approach has proven effective mainly under the operative conditions considered in the design of the blade whereas it is not effective in off-design conditions.

Due to the relationship between blade flap oscillation and noise intensity, a reduction of the flap excursion through harmonic control has been tried as a mean to reduce the intensity of emission.[9, 10] This class of solutions, based on the application of a suitable pitch control action targeting prescribed per-rev harmonics in the blade displacement signal, does not bear completely successful results in term of noise containment, due to the fact that the noise intensity perceived on the ground is bound to the orientation of the helicopter and other flight mechanics parameters, besides depending on blade flap motion and blade aerodynamic characteristics.

More recent research efforts have shown that it is possible to effectively relate the noise intensity measured on the ground to three aero-mechanical parameters,[11, 12] the tip-path plane angle of attack α_{TPP}, the thrust coefficient C_T and the tip speed ratio μ. It has been shown that a database of emission intensities associated to the hemisphere under the rotor can be parameterized with respect to these parameters when executing an approach maneuver with a prescribed profile.[13–15] This database can be pre-computed through numerical simulations or through a mixed numerical-empirical method. The availability of such database enables the setup of an on-board noise estimator, which

from the knowledge of all the three parameters should ideally select the noise intensity distribution over the hemisphere under the rotor, from which the noise footprint on the ground can be obtained.

To this time, the difficulties in practically measuring the required parameters α_{TPP} and C_T limits the use of this technique.

In this paper we present a novel method to estimate the parameters α_{TPP} and C_T from a set of basic measures typically available on most helicopters, augmented by a measurement of the flapping motion of the blades, in the form of the cone angle and of the 1/rev (one per rotor revolution) amplitude and phase of the flap angle. The MANOEUVRES project[16,17] is actively working to the design of an innovative sensor system able to accurately and reliably measure the flap motion of the blades. Preliminary testing on this sensor system have given positive results, addressing the potential problem of obtaining the necessary measures of flap motion.

At this stage of the research we concentrate on the noise prediction in terminal maneuvers, which are among the most relevant in terms of noise effects due to the slow motion of the helicopter and ensuing high intensity BVI-induced noise, and to the proximity with the ground. For this reason, the results proposed in the closing sections of the paper are mainly related to a basic landing maneuver, assumed as design condition. Further results assess the goodness of the proposed observer with respect to off-design conditions, hence paving the way for the development of a more complete methodology for noise prediction: provided a more general database was available, the observer would enable its use by measuring the necessary parameters not only during landing but in more general flight conditions.

2. OBSERVER STRUCTURE: THE EQUATION OF THE FLAPPING BLADE

In order to postulate the structure of an observer for a set of desired aero-mechanical quantities based on the knowledge of an assigned set of measures, it is useful to study what relationship exist between these sets of variables.

The equation for the flapping blade, which will be briefly recalled in this paragraph, provides a comprehensive view of the relationships between the variables defining the state of the helicopter from the viewpoint of flight mechanics and those characterizing the flap-wise motion of the blade. A full description of the passages in the derivation process which are not shown in this pa-
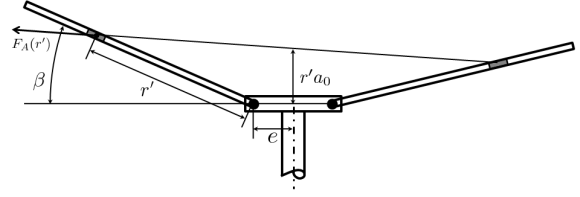
Figure 1: Sketch of the configuration of a flapping rotor.

per can be found in Ref. 18.

2.1. Moment equilibrium at the blade hinge

An expression for the dynamic equilibrium of a flapping blade can be obtained by equating to zero the sum of the differential contributions to the hinge moment due to centrifugal effect, inertia, aerodynamics and weight. The derivation process can be carried out in terms of azimuth ψ instead of explicitly in time domain, due to the stationary rotational speed Ω of the rotor, yielding the equivalence $d\psi = \Omega dt$. The approach presented in the following can be applied to both articulated and hingeless rotor configurations, considering that in the latter case the reaction due to the stiffness of the blade is usually small with respect to all other effects. A general case where the rotor features a hinge offset with respect to the axis of rotation will be considered here. Refer to the the rotor geometry presented in Fig. 1, where e is the dimensional hinge offset, β the flap angle, defined between a plane normal to the axis of the mast and the blade, and r' is the coordinate of the generic blade station measured along the blade axis from the hinge point.

Assuming a flap solution composed of a constant cone term and a 1/rev oscillating term with its phase, as in

$$
\text{(1)} \qquad \beta = a_0 - a_1 \cos\psi - b_1 \sin\psi
$$

and a small-angle scenario such that the centrifugal force be acting in a plane parallel to the tip-path-plane, instead of being normal to the direction of Ω, the contribution to the hinge moment due to the centrifugal effect can be written as

$$
M_C =
$$

$$
\text{(2)} \quad = -\Omega^2 \left\{ a_0 \int_0^{R-e} mr'(r'+e)dr - (a_{1_s}\cos\psi + \right.
$$

$$
\left. + b_{1_s}\sin\psi)e \int_0^{R-e} mr'dr \right\}
$$

By substituting the definitions for the static moment $\frac{M_b}{g} = \int_0^{R-e} mr'dr$ and moment of inertia $I_b = \int_0^{R-e} mr'^2 dr$ for the flapping section of the blade, Eq. 3 can be rewritten as

(3)
$$M_C =$$
$$= -\Omega^2 \left\{ a_0(I_b + e\frac{M_b}{g} - (a_{1_s}\cos\psi + b_{1_s}\sin\psi)e\frac{M_b}{g} \right\}$$

Considering the contribution to the hinge moment due to aerodynamics, for the generic blade station of span dr' at a distance r' from the hinge it is possible to write

(4)
$$\Delta M_A = r'\frac{\rho}{2}U_T^2 a\,\alpha\,c\,dr'$$

where ρ is air density, a the slope of the linear portion of the lift curve of the blade profile, c the chord of the profile. Furthermore, the tangential (i.e. normal to the rotor axis) speed experienced by the blade station is

(5)
$$U_T = \Omega R \left(\frac{r'+e}{R} + \mu\sin\psi \right)$$

wherein $\mu = \frac{V}{\Omega R}$ is the tip speed ratio, and the expression of the speed shows a contribution due to the rotation of the rotor and another due to the translational motion of the helicopter.

The value of α in Eq. 4 can be defined from the sum of pitch θ and of the ratio of the speed component aligned with the rotor axis U_P to the tangential speed U_T.

The pitch angle can be hypothesized to be composed of a collective component θ_0, a constant component due to twist θ_1 and an 1/rev oscillating cyclic component, as in the expression

(6)
$$\theta = \theta_0 + \theta_1\frac{r'}{R} - A_1\cos\psi - B_1\sin\psi$$

The value of the component of the air speed field locally aligned with the rotor axis can be expressed as a function of the flap angle, the angle of attack of the tip-path plane α_{TPP} and the inflow speed v_1, as

(7)
$$U_P = \Omega R \{\mu(\alpha_{\text{TPP}} - B_1 + a_{1_s}) +$$
$$-\frac{v_1}{\Omega R}(1 + \frac{r'}{R}\cos\psi) +$$
$$-\frac{r'}{R}(a_{1_s}\sin\psi - b_{1_s}\cos\psi) +$$
$$-\mu(a_0 - a_{1_s}\cos\psi - b_{1_s}\sin\psi)\cos\psi\}$$

In Eq. 7 the relationship between the angle of attack of the tip-path plane and the angle of attack of the swash plate α_s which is more common to find in the literature, yielding $\alpha_s = \alpha_{\text{TPP}} - (B_1 + a_{1_s})$, has been exploited.

Eq. 4 can be integrated over the span of the flapping portion of the blade. Due to the structure of that equation, multiple higher-order harmonic terms are obtained in the expression of the overall aerodynamic moment M_A. It can be hypothesized without a significant loss of accuracy that only constant and 1/rev terms should be retained, or analytically

(8)
$$M_A = M_{A_0} + M_{A_{\sin}}\sin\psi + M_{A_{\cos}}\cos\psi$$

In order to cut on the length of the derivation, the expressions for M_{A_0}, $M_{A_{sin}}$ and $M_{A_{cos}}$ will not be written explicitly, but will be shown as contributions in the final expressions presented at the end of the process.

Finally, the contribution of weight to hinge moment can be written as

(9)
$$M_W = -M_b = -\int_0^{R-e} mgr'dr$$

From equations 3, 8 and 9 it is possible to observe that all three contributions to the expression of equilibrium at the hinge point are composed of a constant and, in the case of the first two, two 1/rev oscillating terms. It is possible to obtain an expression of equilibrium by equating to zero these harmonic components one by one.

Starting from the constant component, it is possible to express the corresponding equilibrium equation as

(10)
$$M_{C_{\text{const}}} + M_{A_{\text{const}}} + M_{W_{\text{const}}} = 0$$

or equivalently
(11)
$$a_0 =$$
$$= \frac{\frac{1}{6}\rho acR^4\left(1 - \frac{e}{R}\right)^2}{I_b + e\frac{M_b}{g}}\left[\theta_0\left(\frac{3}{4} + \frac{3}{4}\mu^2\right) + \theta_1\left(\frac{3}{5} + \frac{\mu^2}{2}\right) +\right.$$
$$\left. +\mu\left(\alpha_{\text{TPP}} - 2B_1 - a_{1_s}\right) - \frac{v_1}{\Omega R}\right] - \frac{M_b}{\Omega^2\left(I_b + e\frac{M_b}{g}\right)}$$

From the basic blade element momentum theory it is possible to obtain the non-dimensional expression for the rotor thrust, yielding

(12)
$$C_T = \sigma\left(1 - \frac{e}{R}\right)\frac{a}{4}\left[\theta_0\left(\frac{2}{3} + \mu^2\right) +\right.$$
$$\left. +\theta_1\left(\frac{1}{2} + \frac{\mu^2}{2}\right) + \mu\left(\alpha_{\text{TPP}} - 2B_1 - a_{1_s}\right) - \frac{v_1}{\Omega R}\right]$$

By manipulation of Eq. 11 and 12, an expression of equilibrium related to the non oscillating component of the hinge moment can be written as

$$(13) \qquad a_0 = \frac{\frac{2}{3}\rho c R^4 \left(1 - \frac{e}{R}\right)\frac{C_T}{\sigma}}{I_b + e\frac{M_b}{g}} - \frac{M_b}{\Omega^2 \left(I_b + e\frac{M_b}{g}\right)}$$

With a similar procedure it is possible to obtain the expressions of equilibrium corresponding to the 1/rev oscillating component of the hinge moment, which is represented by equations

$$(14) \qquad \begin{aligned} M_{C_{\sin_{1/rev}}} + M_{A_{\sin_{1/rev}}} &= 0 \\ M_{C_{\cos_{1/rev}}} + M_{A_{\cos_{1/rev}}} &= 0 \end{aligned}$$

It should be noted that only the aerodynamic and centrifugal terms have an effect on the pulsating component of the hinge moment, whereas the weight term has an effect only in the equation derived for the constant component a_0. By substitution of the respective terms in Eq. 14 the expression for the sine yields

$$(15) \qquad \begin{aligned} &\Omega^2 b_{1_s} e \frac{M_b}{g} + \frac{\gamma I_b}{2}\Omega^2 \left(1 - \frac{e}{R}\right)^2 \left[\frac{2}{3}\theta_0\mu + \frac{1}{2}\theta_1\mu + \right. \\ &- B_1 \left(\frac{1}{4} + \frac{3}{8}\mu^2\right) + \\ &+ \frac{\mu}{2}\left(\mu\left(\alpha_{\mathsf{TPP}} - B_1 - a_{1_s}\right) - \frac{v_1}{\Omega R}\right) \\ &\left. - a_{1_s}\left(\frac{1}{4} - \frac{\mu^2}{8}\right)\right] = 0 \end{aligned}$$

whereas that for the cosine yields
(16)
$$\begin{aligned} &\Omega^2 a_{1_s} e \frac{M_b}{g} + \frac{\gamma I_b}{2}\Omega^2 \left(1 - \frac{e}{R}\right)^2 \left[-A_1\left(\frac{1}{4} + \frac{\mu^2}{8}\right) + \right. \\ &\left. - \frac{a_0\mu}{3} - \frac{1}{3}\frac{v_1}{\Omega R} + b_{1_s}\left(\frac{1}{4} + \frac{\mu^2}{8}\right)\right] = 0 \end{aligned}$$

The parameter $\sigma = \frac{cN_b}{\pi R}$ is the solidity of the rotor, where N_B is the number of blades, and $\gamma = \frac{\rho a c R^4}{I_b}$ is the Lock number.

These equations have a general validity in advanced, symmetric flight, hence they can be assumed to describe with an acceptable accuracy for the scope of the present analysis the conditions of the blade in a standard approach maneuver. Further usual hypotheses that have been implicitly assumed are linear aerodynamics and no reverse flow region on the rotor.

2.2. Structure of the observation model

Equations 13, 15 and 16 can be used to obtain the amplitudes of the flap response a_0, a_{1_s} and b_{1_s}, i.e. a solution for the flap-wise motion, in case all other parameters are known. On the other hand, in the present analysis the same equations can be manipulated in order to find an expression for α_{TPP} as a function of the other parameters, especially the coefficients of the flapping solution, which are supposed to be known in the scenario of interest here.

To this aim, it should be observed that the quantity α_{TPP} does not show up in Eq. 13, whereas C_T does. Furthermore, both equations 15 and 16 show a dependence on α_{TPP} and on the inflow speed v_1. The latter is instrumental in the definition of the induced speed $V_L = v_1(1 + \frac{r}{R}\cos\psi)$, which has been used in Eq. 7.

An expression for v_1 can be driven from the momentum theory, yielding a relationship between this parameter and C_T in the form

$$(17) \qquad \frac{v_1}{\Omega R} = \frac{C_T}{2\mu}$$

The inflow term $\frac{v_1}{\Omega R}$ can be substituted by a function of C_T and μ exploiting Eq. 17 in Eq. 15 and 16. An effect of this substitution is that all three equations obtained from hinge moment equilibrium show a dependence on the parameter C_T, which is usually not directly measurable. This dependence highlights the fact that the problem of observation of α_{TPP} is coupled with that of C_T.

In order to observe these two quantities it is possible to exploit two of the three equations for flapping equilibrium. Moreover, by inspection of Eq. 13 it is possible to notice that only C_T shows up in that expression, suggesting a possible triangular coupling in the observation problem of α_{TPP} and C_T.

The shape of the observation model can be investigated starting from Eq. 13, which can be rewritten as

$$(18) \qquad C_T = \frac{\sigma\left\{\left(I_b + e\frac{M_b}{g}\right)a_0 + \frac{M_b}{\Omega^2}\right\}}{\frac{2}{3}\rho c R^4\left(1 - \frac{e}{R}\right)}$$

Similarly, Eq. 15 can be rearranged as follows

$$(19) \qquad \begin{aligned} &\frac{\mu^2}{2}\alpha_{\mathsf{TPP}} - \frac{1}{4}C_T = \\ &= \left(\frac{3}{8}\mu^2 + \frac{1}{4}\right)a_{1_s} - \left(\frac{2eM_b}{g\gamma I_b\left(1 - \frac{e}{R}\right)^2}\right)b_{1_s} + \\ &- \frac{2}{3}\mu\theta_0 - \frac{1}{2}\mu\theta_1 + \left(\frac{7}{8}\mu^2 + \frac{1}{4}\right)B_1 \end{aligned}$$

Equations 18 and 19 considered together suggest the structure of the observation model for α_{TPP} and C_T, which can be formalized as follows

(20)
$$Qs = \tilde{T}m + \tilde{q}$$

where array $s^T = \{\alpha_{\text{TPP}}, C_T\}$ includes the quantities to be observed and array $m^T = \{a_0, a_{1_s}, b_{1_s}, \theta_0, B_1\}$ is made of the measures necessary for the observation. The coefficients of the matrices Q and $\tilde{T}$ and of the array $\tilde{q}$ can be obtained from Eq. 18 and 19 as

$$Q = \begin{bmatrix} \frac{\mu^2}{2} & -\frac{1}{4} \\ 0 & 1 \end{bmatrix}$$

(21)
$$\tilde{T} = \begin{bmatrix} 0 & \left(\frac{3}{8}\mu^2 + \frac{1}{4}\right) & \cdots \\ \frac{\sigma(I_b + e\frac{M_b}{g})}{\frac{2}{3}\rho cR^4(1 - \frac{e}{R})} & 0 & \cdots \end{bmatrix}$$

$$\begin{bmatrix} \cdots & -\left(\frac{2eM_b}{g\gamma I_b(1-\frac{e}{R})^2}\right) & -\frac{2}{3}\mu & \left(\frac{7}{8}\mu^2 + \frac{1}{4}\right) \\ \cdots & 0 & 0 & 0 \end{bmatrix}$$

$$\tilde{q} = \left\{ \begin{array}{c} -\frac{1}{2}\mu\theta_1 \\ -\frac{\sigma\frac{M_b}{\Omega^2}}{\frac{2}{3}\rho cR^4\left(1-\frac{e}{R}\right)} \end{array} \right\}$$

From the definition of matrix Q it is clear that no singularity can be expected unless $\mu = 0$, which happens only for hover conditions. As a consequence it is always possible to left-multiplying Eq. 20 by the inverse of Q, yielding

(22)
$$s = Tm + q$$

where $T = Q^{-1}\tilde{T}$ and $q = Q^{-1}\tilde{q}$. Equation 22 with matrices 21 clearly indicates a structure for the proposed observer. The coefficients of the model matrix T and q depend largely on constant geometrical and inertial properties of the considered helicopter rotor, namely through I_b, M_b, σ, e, c and R. Furthermore, they are functions of air speed – through the tip speed ratio μ – and altitude – both explicitly through ρ and through the Lock number γ.

Both speed and altitude may vary during the approach maneuvers of interest here. In this respect, in the results section it will be shown that the effect of changes in the values of both quantities suggests that even significantly different altitude values produce a small change on the coefficients of the model matrices, whereas the effect of air speed is much more pronounced. Following this assumption the dependence of the model coefficients from altitude can be neglected, yielding the expression $T = T(\mu)$ and $q = q(\mu)$.

An important remark concerns the values of the coefficients of the control solution θ_0 and B_1 appearing in the

measures. It is possible to reduce the size of the array of necessary measurements m under the hypothesis of trimmed flight, which from the viewpoint of hinge equilibrium translates into a relationship between the coefficients just mentioned and the values of the coefficients of the flap response a_0, a_{1_s} and b_{1_s}. If the maneuver can be assumed to be quasi-static, no significant dynamic phenomena should show up in the flap-wise motion of the blades either. For the standard approach maneuver considered here it can be safely assumed that the helicopter is moving in a trimmed flight condition. This in turn allows to hypothesize that there exist a relationship between the coefficients of the trimmed pitch input and those of the flap-wise deflection. This remark yields a reduction of the array of measures to $m^T = \{a_0, a_{1_s}, b_{1_s}\}$.

In conclusion, what is suggested by the theory is a structure of the observation model in the explicit form

(23)
$$\left\{ \begin{array}{c} \alpha_{\text{TPP}} \\ C_T \end{array} \right\} = T(\mu) \left\{ \begin{array}{c} a_0 \\ a_{1_s} \\ b_{1_s} \end{array} \right\} + q(\mu)$$

Further slight alterations to the model structure in Eq. 23 will be presented in the result sections based on performance advantages suggested by practical evidence.

Provided all quantities explicitly reported in Eq. 21 are known with sufficient accuracy, it could be possible to find the coefficients of the model through their respective definitions. An alternative approach through parameter identification has been considered here to find the required model coefficients. Details on the identification process will be provided in the next section.

It should be remarked that, besides making unnecessary the computation of all quantities appearing in the definitions in Eq. 21, an approach through model identification allows the synthesis of a model better tailored to the dataset used for identification. Provided the identification campaign is properly planned to cover all operative conditions of interest, the hypothesized model structure is such to capture the essence of the relationship between the measures and the observed signals, and if the identification algorithm is suitable for the considered problem, the accuracy of the model coefficients with respect to the testbed is usually higher than what can be obtained through purely analytic estimation.[19]

3. SYNTHESIS OF THE OBSERVATION MODEL: APPROACH THROUGH PARAMETER IDENTIFICATION

In order to compute the coefficients of the proposed model in Eq. 23, an approach based on model identification has been developed, based on the procedure proposed in Ref. 19 and references therein.

On account of the dependence of the observation model on parameter μ the coefficients of the observation model can be found for an assigned speed $\bar{V}$ of the slipstream, and correspondingly for a given $\bar{\mu}$. In order to identify the model matrix of a linear model $\boldsymbol{T}(\bar{\mu})$ it is necessary to collect time samples composed of measures of the quantities to be observed s_i and of the measures m_i intended for feeding the observer. Furthermore, the identification of the coefficients of $\boldsymbol{q}(\bar{\mu})$ can be carried out by augmenting the array of measurements with a unitary element and performing the identification on a homogeneous system structure. To this aim the model matrix of the homogeneous system can be defined as $\boldsymbol{K}(\bar{\mu}) = [\boldsymbol{T}(\bar{\mu})\,\boldsymbol{q}(\bar{\mu})]$.

In practice, in order to deal with changing values of the parameters – including air speed – during simulations, it was decided to distribute the samples composing the time histories of the signals measured in the simulation runs performed for identification based on their respective air speed values into pre-determined speed buckets. Such buckets are centered in N_v equally spaced speed poles, each corresponding to an assigned speed of the stream $\bar{V} = V_p$, and feature an amplitude $\Delta V = \frac{1}{2}(V_{p+1} - V_{p-1})$, so that buckets do not overlap. All samples attributed to a certain air speed bucket will contribute to the identification of the model corresponding to the reference air speed $\bar{V} = V_p$ and the corresponding $\bar{\mu}_p$.

Collecting the values of $\boldsymbol{s}_i^T = \{\alpha_{\text{TPP}_i}, C_{T_i}\}$ and $\boldsymbol{m}_i^T = \{a_{0_i}, a_{1_{s_i}}, b_{1_{s_i}}, 1\}$ for $i = 1, \cdots, N_p$, where N_p is the number of considered samples for the assigned $\bar{\mu}$, the homogeneous model matrix $\boldsymbol{K}(\bar{\mu}_p)$ will be such that

$$(24) \qquad \begin{bmatrix} \boldsymbol{s}_1 \cdots \boldsymbol{s}_{N_p} \end{bmatrix} = \boldsymbol{K}(\bar{\mu}_p) \begin{bmatrix} \boldsymbol{m}_1 \cdots \boldsymbol{m}_{N_p} \end{bmatrix}$$

This can be rewritten synthetically as

$$(25) \qquad \boldsymbol{S} = \boldsymbol{K}(\bar{\mu}_p)\boldsymbol{M}$$

The values of the coefficients of the model matrix for the assigned $\bar{\mu}$ can be obtained through a suitable identification method. For the problem under analysis a least-squares method has been deemed satisfactory. This yields

$$(26) \qquad \hat{\boldsymbol{K}}(\bar{\mu}_p) = \boldsymbol{S}\boldsymbol{M}^T(\boldsymbol{M}\boldsymbol{M}^T)^{-1}$$

where the $\hat{(\cdot)}$ sign indicates that the coefficients have been estimated.

Once the coefficients of the model matrix are known, matrix $\hat{\boldsymbol{K}}(\bar{\mu}_p)$ can be used online for obtaining an estimation of the desired quantities $\hat{s}$ from a measurement of the parameters $\boldsymbol{m}$

$$(27) \qquad \hat{s} = \hat{\boldsymbol{K}}(\bar{\mu}_p)\boldsymbol{m}$$

In order to make use of the observer in an operational condition featuring a changing value of the tip speed ratio μ it is necessary to preliminarily store the values of the coefficients for a suitable number of operational conditions each characterized by a value $\bar{\mu}_p$, covering the operational speed envelope of the helicopter in the considered class of maneuvers (approach and landing). The corresponding model matrices will be interpolated online based on the actual value of the tip speed ratio. In this work a linear interpolation was considered between identification nodes, yielding

$$(28) \qquad \begin{aligned} \boldsymbol{K}(\mu) =& \boldsymbol{K}_p + (\boldsymbol{K}_{p+1} - \boldsymbol{K}_p)\frac{\mu - \bar{\mu}_p}{\bar{\mu}_{p+1} - \bar{\mu}_p}, \\ & \bar{\mu}_p \le \mu < \bar{\mu}_{p+1} \end{aligned}$$

for the model matrix related to the actual value of μ.

As highlighted in the previous section, in the result section it will be shown that the array of measurements $\boldsymbol{m}$ can be modified with respect to what is suggested by theory to improve the results, but the identification procedure presented in Eq. 24, 25 and 26 can be left unchanged.

4. RESULTS

In this section the feasibility of the proposed observer will be demonstrated at first showing the quality of the identified model and successively the accuracy in the estimation of α_{TPP} and C_T, both in design and off design conditions. All results proposed in this section have been obtained working with `RSim`,[20,21] a code for simulation of the flight mechanics of helicopters based on the formulation of Ref. 22, with a built-in model for the flapping blade, which allows to compute individually the amplitude of the cone and 1/rev sine and cosine components of the flap-wise deflection. The simulator implements models for dynamic inflow and wake. The considered model of helicopter represents an existing machine, and features a four-bladed, hingeless rotor and a conventional tail rotor configuration. The `RSim` code integrates the trajectory of the helicopter, which is controlled in closed loop through collective, longitudinal

and lateral pitch of the main rotor, and collective pitch of the tail rotor.

As mentioned in the introduction, the design condition for this analysis is that of a symmetric, straight approach maneuver. The maneuver has been repeated for parameterized values of some design parameters. The starting altitude is $h_{in} = 3000$ ft. Values of the initial speed of the helicopter V_{in} of 30 to 50 kn every 10 kn have been considered. The helicopter is assumed to travel the descent trajectory in unaccelerated flight. Five glide-slope angles between 3 to 7 deg every 1 deg have been considered. Finally, the helicopter is stabilized in horizontal flight after reaching the final altitude $h_{fin} = 500$ ft.

The mass of the helicopter has been considered constant for the first analyses, as will be illustrated in the following. Successively, this quantity has been considered as a parameter, and all considered simulations have been carried out with a weight value between $68\%W_{ref}$ and $100\%W_{ref}$ with $3.2\%W_{ref}$ increments, W_{ref} being the vehicle reference weight.

The time length of the simulations is in the order of the hundreds of seconds, the exact value depending on the speed and angle of descent, the start and final altitudes being fixed parameters. The data sampling frequency is 0.5 Hz. As a result of the parameterization, a total number of 150 simulations have been considered. Notwithstanding the relatively low number of simulations, the total number of samples and conditions analyzed is significantly high and suitable for identification purposes.

4.1. Identification and model quality

The presence of a realistic control system simulating the action of the pilot in the control loop results in not perfectly constant values of the air speed and in disturbances to other machine states. This condition can be effectively dealt with by distributing the time samples in speed buckets as previously shown. Three wind speed buckets corresponding to V_b of 30, 40 and 50 kn have been considered. All samples from simulations run with a weight of $94\%W_{ref}$ and the considered reference wind speeds of V_{in} of 30 to 50 kn every 10 kn have been attributed to the respective buckets, and the coefficients of a model matrix $\boldsymbol{K}(\bar{\mu}_b)$ have been computed for the value of $\bar{\mu}_b$ corresponding to each V_b.

The model shape considered is that suggested by theory and presented in Eq. 23, accounting for a_0, a_{1_s} and b_{1_s} among the measurements, and where the model matrix is scheduled with respect to the advance ratio μ.
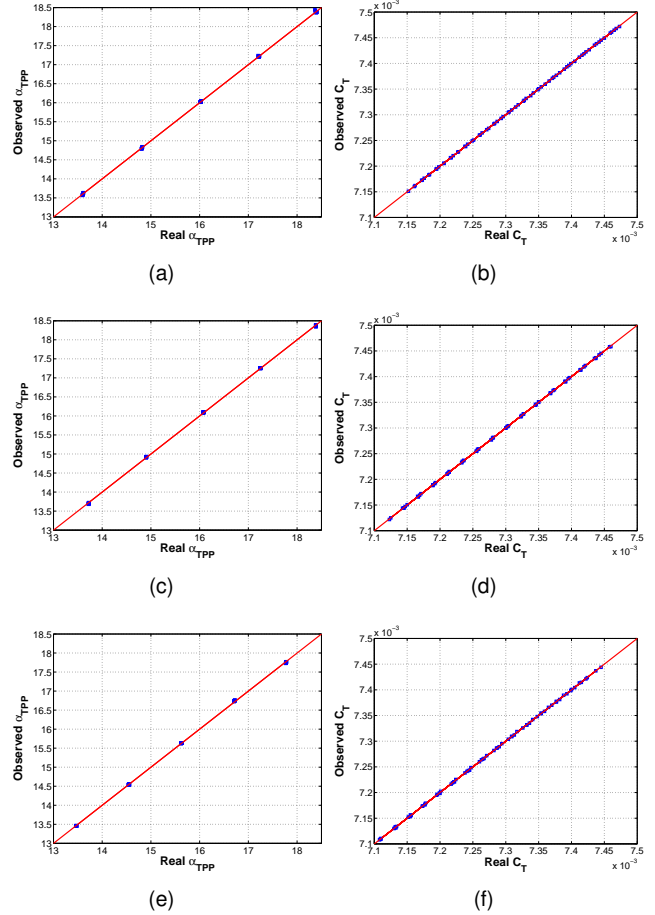
Figure 2: Model quality check for α_{TPP} (left) and C_T (right). Top row: $V_b =$30 kn, mid row: $V_b =$40 kn, bottom row: $V_b =$50 kn. Red line: ideal correlation. Blue squares: results from sampled time histories.

In order to check the identifiability of the parameters of the proposed observer structure, once the model matrix have been computed it is possible to use it on the same pool of measures used for identification to perform an observation. If the model matrix that has been identified is of good quality, the real and observed values of the quantity of interest should lie very close to one another, or ideally be identical.

In Fig. 2 it is possible to see the result of such check for the three considered models, corresponding to three air speeds. The pictures to the left show the result of the check on α_{TPP} and those to the right the result on C_T. On the horizontal axis the real value of the quantity of interest is plotted for each sample, whereas on the vertical axis the corresponding observation value is reported. The red solid line represents the ideal 1:1
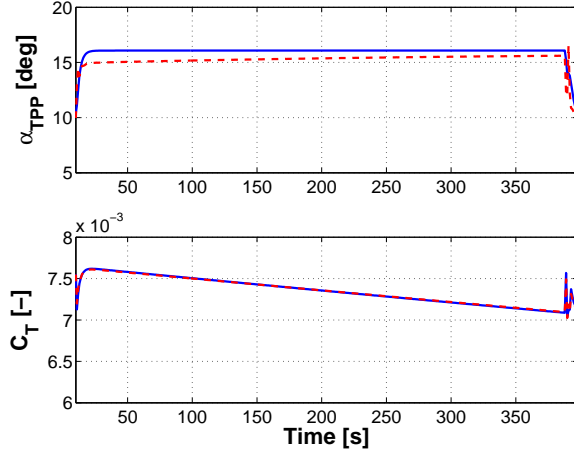
Figure 3: Time histories of real and observed values of α_{TPP} (top) and C_T (bottom). Blue solid line: real values. Red dashed line: observed values. 5 deg glide slope, airspeed 40 kn.

Figure 4: Average relative error for simulations at various speeds and glide-slope angles. Observer checked on the same samples considered for identification. Left bars: α_{TPP}, right bars: C_T.

correlation between the real value and the observation. The quality of the observer matrix can be assessed based on the distance between the ideal line and the blue squares, each representing a sample. In this and all similar figures in this paper, only one sample every 100 in a simulation have been considered for plotting, to make pictures clearer.

From Fig. 2 it can be seen that the quality of the model is generally good on both α_{TPP} and C_T, although visibly better on C_T. This is in accordance with the presented model (Eq. 21), where C_T shows an analytically simpler dependence on a smaller set of measures with respect to α_{TPP}, favoring the ease of observation and observation accuracy.

An example of the time histories of the real and observed values of α_{TPP} and C_T is presented in Fig. 3.

In Fig. 4 the value of relative error for the three buckets and respective model matrices $\boldsymbol{K}(\mu_b)$, $V_b = 30,\ 40,\ 50$ kn is shown for the same conditions of Fig. 2. The presented values of the error have been computed as in Eq. 29,

$$(29) \qquad E_p = \frac{1}{N_p} \sum_{i=1}^{N_p} \frac{\sqrt{(\boldsymbol{s}_i - \hat{\boldsymbol{K}}(\mu)\boldsymbol{m}_i)^2}}{\boldsymbol{s}_i}$$

The left bars in the figure refer to α_{TPP}, the right bars to C_T. From Fig. 4 the higher value of the error on α_{TPP} is apparent. Both errors are considerably low, suggesting a very high accuracy of the observation, which is

clearly auspicable in the case of this first check on the identifiability of the model.

4.2. Improvements to the model structure

As anticipated in the section devoted to the description of the model structure, the model matrix in Eq. 21 depends only on μ, whereas the matrices in Eq. 21 obtained from theory suggest a dependence both on the tip speed ratio μ and on altitude, both explicitly through ρ and through the Lock number γ, itself a function of ρ.

The actual dependence of the model matrices obtained through identification on both μ and ρ have been analyzed by considering ad hoc identification processes carried out respectively in constant-altitude, variable-speed and in variable-altitude, constant-speed conditions.

Examples of results are shown in Fig. 5. The bar plot on the left shows the effect of changing speed on the coefficient of the model matrix, for a constant altitude of 2000 ft, whereas the bar plot to the right reports the change of the model coefficients for changing altitudes and a fixed speed of 40 kn. Both figures refer to results obtained considering a constant weight of 94%W_{ref}. Top plots refer to the coefficients relating α_{TPP} to the measures, bottom plots refer to the coefficients for C_T. The considered coefficients are four, accounting for the the three multipliers of the measures and for the constant term in $\boldsymbol{q}$. The coefficients are normalized with respect to their corresponding values at minimal speed and minimal altitude, on the left and
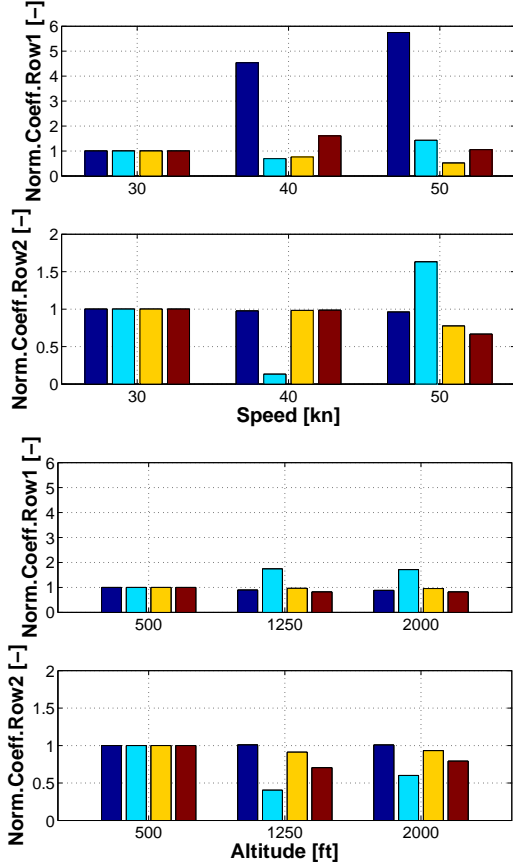
Figure 5: Normalized change in model coefficients. Top plots: dependence on speed at fixed altitude of 2000 ft for the model coefficients for α_{TPP} and C_T. Bottom plots: dependence on altitude at fixed speed of 40 kn for the same coefficients.

right plots respectively. This normalization yields unitary values on the leftmost columns on each plot.

From Fig. 5 it can be argued that the effect of changing speed is more marked than that of altitude. This justifies the assumption that $\boldsymbol{K} = \boldsymbol{K}(\mu)$. This model structure is simpler to treat from the viewpoint of identification than one where $\boldsymbol{K}$ is a function of multiple parameters, requiring a less extensive group of simulations for identification.

Despite the more relevant effect of speed, Fig. 5 shows that also altitude bears an effect on the coefficients of the model. In order to account for this dependency in an easy way, density ρ has been included in the array of measurements. This choice, although not explicitly supported by the theoretical model presented above, can be justified empirically on the basis of an improved model quality. It corresponds to considering altitude as
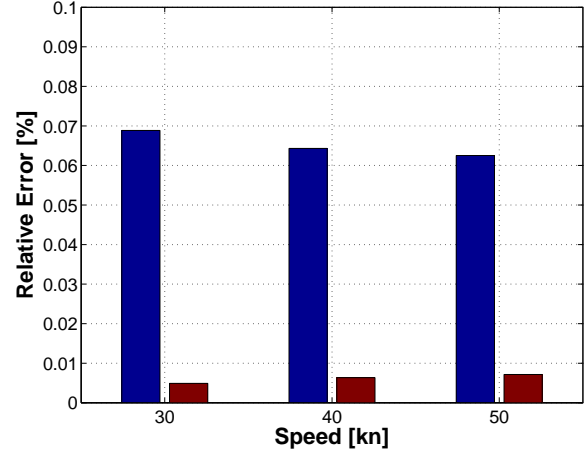
Figure 6: Average relative error for simulations at various speeds and glide-slope angles. Observer checked on the same samples considered for identification. Left bars: α_{TPP}, right bars: C_T. Theoretical measurement array augmented with density ρ.

a measurable disturbance. The relative observation error for a model where the array of measurements is composed of $\boldsymbol{m} = (a_0, a_{1_s}, b_{1_s}, \rho)^T$ and computed on the same conditions considered for the results in Fig. 4 is presented in Fig. 6. By comparing the two figures it is possible to notice a slight reduction in the relative error.

Similarly, an effect which is not included explicitly in the theoretical model is that of the weight of the helicopter. This can be assumed constant during an approach maneuver, yet its effect on the coefficients of the model needs to be investigated due to the potential significant change in the value of this quantity for different flight configurations (number of passengers, residual fuel, etc.). The relevance of weight on the quality of identification can be shown by considering a set of simulations where speed changes between 30 and 50 kn and all previously assumed glide-slope angles have been considered, whereas multiple values of the weight are considered, varying between $68\%W_{\mathsf{ref}}$ and W_{ref} every $3.2\%W_{\mathsf{ref}}$ as mentioned at the beginning of this section. Figure 7 illustrates the relative error in case weight is not included in the measures (left), so that $\boldsymbol{m} = (a_0, a_{1_s}, b_{1_s})^T$, and in case it is (right), yielding $\boldsymbol{m} = (a_0, a_{1_s}, b_{1_s}, W)^T$.

Based on the performance advantages briefly summarized through the figures above, the measurement array can be assumed for the remaining of this section to be composed of $\boldsymbol{m} = (a_0, a_{1_s}, b_{1_s}, \rho, W)^T$. Figure 8 shows
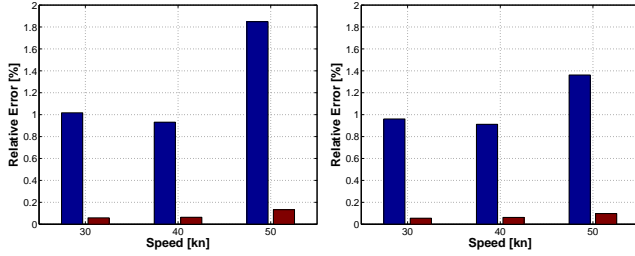
Figure 7: Average relative error for simulations at various speeds, glide-slope angles and helicopter weight. Observer checked on the same samples considered for identification. Left bars: α_{TPP}, right bars: C_T. Left plot: theoretical measurement array. Right plot: theoretical measurement array augmented with helicopter weight W.
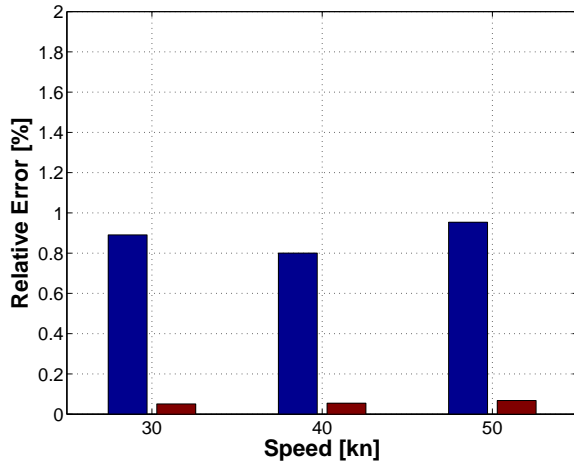
Figure 8: Average relative error for simulations at various speeds, glide-slope angles and helicopter weight. Observer checked on the same samples considered for identification. Left bars: α_{TPP}, right bars: C_T. Theoretical measurement array augmented with density ρ and helicopter weight W.

the relative error of the model obtained considering this array of measurements and the full database of simulations as for Fig. 7.

4.3. Observation results in design conditions

In order to check the quality of the observation algorithm more simulations have been performed at intermediate speeds of 35 and 45 kn, for all the weights and glide-slope angles considered in the observer synthesis process. The model coefficients have been linearly

interpolated as previously explained, as suggested in Ref. 19 and presented in Eq. 28 based on the actual value of the speed of each sample in the new simulations. The augmented array of measurement suggested in the previous paragraph has been considered here.

The results in Fig. 9 follow the same presentation scheme used in Fig. 2. It is possible to notice that the agreement between the real and observed values

(a)

(b)
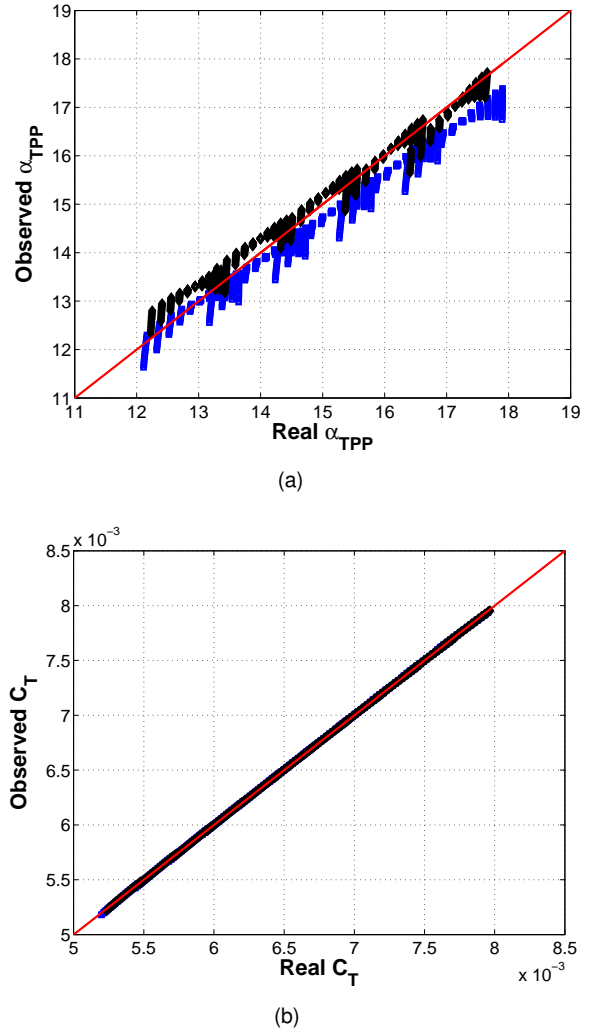
Figure 9: Observation quality check for α_{TPP} (top) and C_T (bottom). Descent maneuvers at 35 and 45 kn, altitudes varying between 3000 and 500 ft, weight varying between $68\%W_{\text{ref}}$ and W_{ref}. Theoretical measurement array augmented with density ρ and helicopter weight W. Red line: ideal correlation. Black diamonds and blue squares: results from sampled time histories at 35 and 45 kn respectively.

is good, both in terms of α_{TPP} and C_T.

The relative error between observation and real value in this case is 1.91% for α_{TPP}, whereas it is 0.0549% for C_T. It can be noted that although clearly higher than in the previous checks on the model, the value of error on both α_{TPP} and C_T remains limited, assuring good accuracy of the observation error even for collected at speeds not considered for model synthesis. Furthermore, recalling that interpolation between precomputed models corresponding to other air speeds has been used for this test, this result suggests that a relatively loose discretization with respect to air speed as the one considered here is enough for obtaining an acceptable level of precision in the observation.

4.4. Observation results in off-design conditions

In order to assess the robustness of the observation algorithm with respect to disturbances further simulations have been run in two scenarios different from that considered for identification. In a first scenario the helicopter is slipping laterally by +/–5 and +/–10 deg, traveling at 50 kn and for the same values of the glide-slope angle and weight considered for identification, yielding a total of additional 220 simulation runs.

Figure 10 shows the observation results pertaining to this scenario. The accuracy is clearly lower than in all previous cases on α_{TPP} (left plot), where the samples lying at the greatest distance below the ideal line refer to a sideslip angle of +5 and +10 deg. A non-linear relationship between the value of sideslip and the considered array of measurements yields a non-symmetric behavior of the observation with respect to the sideslip angle. This is reflected in the non-symmetric disposition of the observation samples, with samples corresponding to negative angular values lying closer to the ideal line than samples corresponding to positive values. On the other hand, the accuracy of the observation of C_T is distinctively better.

The relative error in this scenario is 4.41% for α_{TPP} and 0.363% for C_T. Although higher than before, this error obtained in off-design conditions can be deemed low enough to allow practical use of the observed signals even in presence of a noticeable sideslip disturbance.

Finally, in a second off-design scenario the helicopter has been considered following a decelerated descent trajectory. The initial condition has been set to $V_{in} = 50$ kn and $h_{in} = 3000$ ft and the final condition is $V_{fin} = 30$ kn and $h_{fin} = 500$ ft. Simulations performed at different values of the weight between 68%W_{ref} and 100%W_{ref} every 3.2%W_{ref} have been considered,
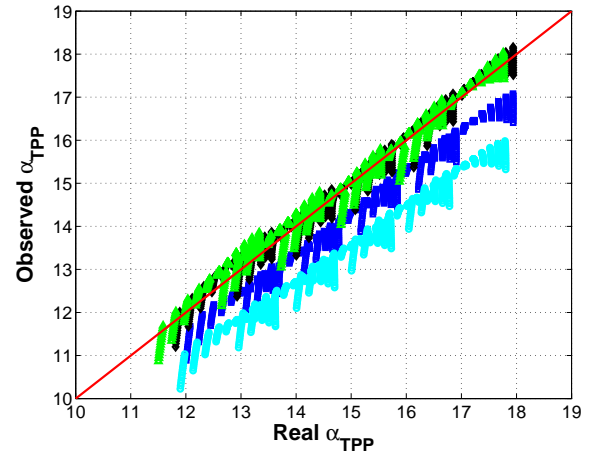
(a)
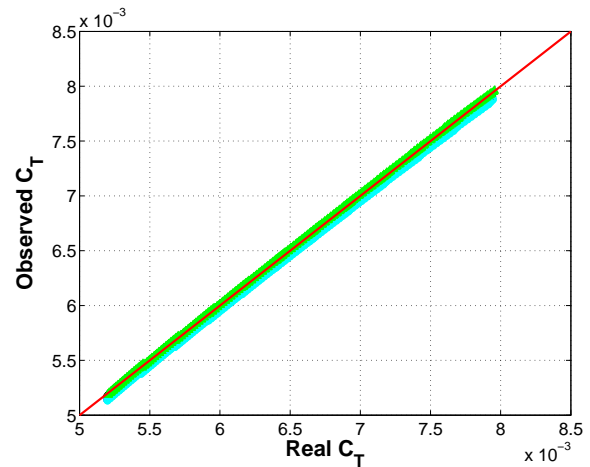
(b)

Figure 10: Observation quality check in presence of a non-null sideslip angle (off-design conditions) for α_{TPP} (top) and C_T (bottom). Descent maneuvers at 50 kn, altitudes varying between 3000 and 500 ft, weight varying between 68%W_{ref} and W_{ref}, at ± 5 and ± 10 deg sideslip angle values. Theoretical measurement array augmented with density ρ and helicopter weight W. Red line: ideal correlation. Blue squares and black diamonds: results from sampled time histories, ± 5 deg sideslip respectively. Cyan rounds and green triangles: results from sampled time histories, ± 10 deg sideslip respectively.

whereas four durations of the descent have been accounted for 300, 350, 400 and 450 s, yielding four different constant descent rates. Due to the time evolution imposed on the total speed of the helicopter and to the constraint on the vertical speed, the glide-slope angle

(a)

(b)
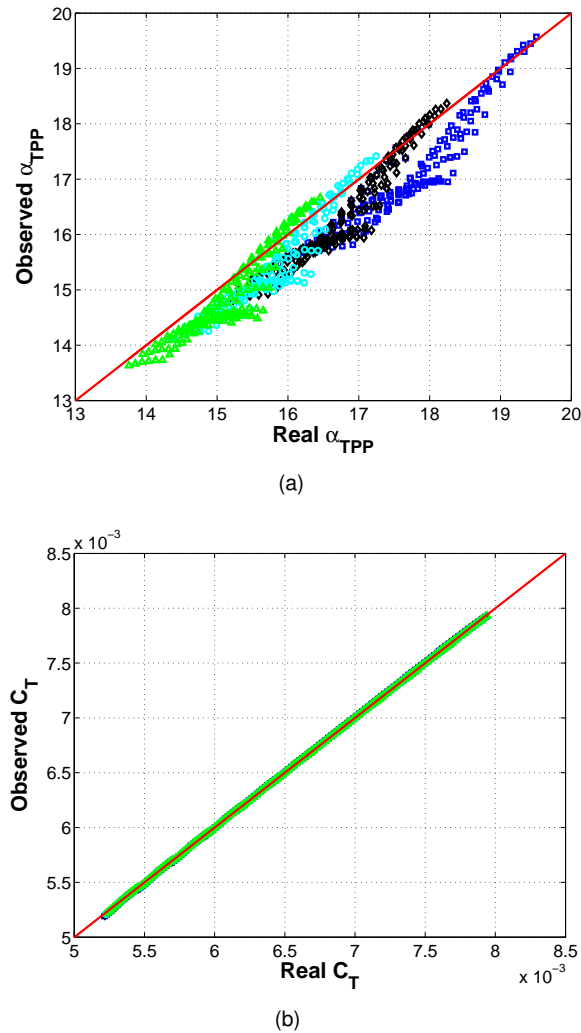
Figure 11: Observation quality check for a decelerated descent (off-design conditions) for α_{TPP} (top) and C_T (bottom). Descent maneuvers starting at 50 kn and ending at 30 kn, altitudes varying between 3000 and 500 ft, weight varying between 68%W_{ref} and W_{ref}. Theoretical measurement array augmented with density ρ and helicopter weight W. Red line: ideal correlation. Blue squares, black diamonds, cyan rounds and green triangles: deceleration in 300, 350, 400 and 450 s, respectively.

is not constant during a simulation.

The results from this scenario are presented in Fig. 11. The accuracy of α_{TPP} observation is still good, being higher in correspondence of the helicopter speed passing in proximity of the focal values for which the observation matrices have been stored. Observation of C_T is still remarkably good.

The value of the relative error is 2.76% for α_{TPP} and 0.0689% for C_T. With respect to the previous off-design scenario, the decelerated trajectory does not bear a so relevant decrease in observation accuracy. This shows that as far as only the variables considered as measurements in the design of the observer – primarily altitude, weight and speed, and as a consequence the coefficients of the flapping solution – are changed during a simulation the quality of observation is not severely affected. It can be reported that a far more pronounced loss of accuracy has been encountered when performing simulations where the air speed is pushed beyond the extreme values considered for the scheduling of the model matrix, suggesting once more that this operation cannot be skipped in the design of the observer.

The scenarios considered for this off-design study are clearly perturbations of the design maneuver. Little can be said of the ability of the observer to deliver a good observation accuracy in a more general maneuver. However, the purpose of the observer is that of providing a measurement during approach and not in a general case. This robustness study confirms the goodness of the results for the case under analysis.

5. CONCLUSIONS

In this work we concentrated on the feasibility of an observer for the angle of attack of the tip-path-plane α_{TPP}, to the aim of enabling the online measurement of the noise footprint during approach maneuvers.

In a first stage a substantial theoretical support for the proposed observer is given by analyzing the equation for the flapping blade for a generic rotor configuration. From the equilibrium solution of this equation obtained under the hypothesis of a solution for the flap angle composed of a constant and 1/rev oscillating term, it is possible to find a relationship between α_{TPP} and C_T, where C_T is the rotor thrust coefficient, and the characteristics of the flapping solution. Furthermore, this relationship is linear considering altitude and speed as constant parameters.

Starting from the shape of the observer suggested by theory, an algorithm based on model identification has been selected to obtain the coefficients of the model. In practice, the testbed for the computation of the required model matrices has been the simulation tool `RSim`. A design approach through model identification has been preferred to a purely analytic computations due to its ability to provide model matrices better tailored to the simulation tool in use.

The model matrices have been obtained at first based on the exact model suggested by theory, showing the feasibility of the proposed observer through an observation check based on an extensive set of ad-hoc runs simulating approach maneuvers performed with at different values of the glide-slope angle, air speed and helicopter weight. Next, some modifications to the original structure of the model have been implemented, based on empirical evidence of an improvement in model accuracy. Following such analyses, the model has been designed as linearly scheduled with respect to air speed, and the array of measurements have been augmented with air density and the weight of the helicopter.

The ability of the proposed observer has been demonstrated in both design and off-design conditions. For the latter, conditions of non-null lateral wind and decelerated descents have been considered. Testing in off-design conditions have shown a predictable, not dramatic decrease in the accuracy of the observer, which should not hamper the usefulness of the observer with respect to the intended scope. On the other hand, a certain sensibility with respect to exogenous parameters suggests a possible need for further augmenting the array of measurements, hence increasing the sensibility of the observer to more variables. However, for this is not suggested by the simplified theoretical model considered in this work, moving to a more complex and more comprehensive model may be necessary for including new measurement variables in the observer structure, at the considerable price of a loss of simplicity, reliability and computational weight in the design phase.

ACKNOWLEDGMENTS

REFERENCES

[1] B.W. Sim, T. Beasman, F.H. Schmitz, and G. Gopalan, In-flight blade-vortex interaction (BVI) noise measurements using a boom-mounted microphone array, Proceedings of the 60th Annual Forum of the American Helicopter Society, Baltimore, MD, June 7–10, 2004.

[2] H. Ishii, H. Gomi, and Y. Okuno, Helicopter flight tests for BVI noise measurement using an on-board external microphone, Technical Report, American Institute of Aeronautics and Astronautics, 2005–6119, Reston, VA, 2005.

[3] H.N. Chen, K.S. Brentner, J.S. Shirey, J.F. Horn, S. Ananthan, and J.G. Leishman, Study of the aerodynamics and acoustics of super-BVI, Proceedings of the 62nd Annual Forum of the American Helicopter Society, Phoenix, AZ, May 9–11, 2006.

[4] F.H. Schmitz, E. Greenwood, R.D. Sickenberger, G. Gopalan, D. Conner, E. Moralez, B.W. Sim, G. Tucker, and W.A. Decker, Measurement and characterization of helicopter noise in steady-state and maneuvering flight, Proceedings of the 63rd Annual Forum of the American Helicopter Society, Virginia Beach, VA, May 1–3, 2007.

[5] K.S. Brentner, and H.E. Jones, Noise prediction for maneuvering rotorcraft, Proceedings of the 6th AIAA/CAES Aeroacoustics Conference, Lahaina, HI, June 12–14, 2000.

[6] R.D. Janakiram, and H. Khan, Prediction and validation of helicopter descent flyover noise, Proceedings of the 56th Annual Forum of the American Helicopter Society, Virginia Beach, VA, May 2–4, 2000.

[7] K.S. Brentner, G.A. Bres, G. Perez, and H.E. Jones, Toward a better understanding of maneuvering rotorcraft noise, Proceedings of the 58th Annual Forum of the American Helicopter Society, Montreal, Canada, 2002.

[8] G.A. Bres, K.S. Brentner, G. Perez, and H.E. Jones, Maneuvering rotorcraft noise prediction, *Journal of Sound and Vibration*, Vol. 39, 2003, pp. 719–738.

[9] T.F. Brooks, E.R. Booth, J.R. Jolly, W.T. Yeager, and M.L. Wilbur, Reduction of blade-vortex interaction noise using higher harmonic pitch control, NASA Technical Memorandum 101624, NASA Langley Research Center, Hampton, VA, 1989.

[10] P. Beaumier, J. Prieur, G. Rahier, P. Spiegel, A. Demargne, C. Tung, J.M. Gallman, Y.H. Yu, R. Kube, B.G. van der Wall, K.J. Schultz, W.R. Splettstoesser, T.F. Brooks, C.L. Burley, and D.D. Boyd, Effect of higher harmonic control on helicopter rotor blade-vortex interaction noise: prediction and initial validation, Proceedings of the

75th Fluid Dynamics Symposium, Berlin, Germany, 1994.

[11] H.N. Chen, K.S. Brenter, S. Anantham, and J.G. Leishman, A computational study of helicopter rotor wakes and noise generated during transient maneuvers, Proceedings of the 61st Annual Forum of the American Helicopter Society, Grapevine, TX, 2005.

[12] A.L. Duc, P. Spiegel, F. Guntzer, M. Lummer, H. Buchholz, and J. Goetz, Simulation of complete helicopter noise in maneuver flight using aeroacoustic flight test database, Proceedings of the 64th Annual Forum of the American Helicopter Society, Montreal, Canada, 2008.

[13] M. Gennaretti, J. Serafini, M. Molica Colella, and G. Bernardini, Simulation of helicopter noise in maneuvering flight, Proceedings of the European Rotorcraft Forum ERF2014, Southampton, UK, September 2–5, 2014.

[14] M. Gennaretti, J. Serafini, G. Bernardini, A. Castorrini, G. De Matteis, and G. Avanzini, Numerical characterization of helicopter noise hemispheres, *Aerospace Science and Technology* (under review).

[15] M. Gennaretti, G. Bernardini, A. Anobile, J. Serafini, L. Trainelli , A. Rolando, A. Scandroglio, and L. Riviello, Acoustic prediction of helicopter unsteady manoeuvres, 41st European Rotorcraft Forum ERF2015, Munich, Germany, 2015.

[16] L. Trainelli, A. Rolando, E. Zappa, S. Manzoni, M. Lovera, M. Gennaretti, G. Bernardini, P. Cordisco, M. Terraneo, E. Vigoni, and R. Grassetti, MANOEUVRES – An effort towards quieter, reliable rotorcraft terminal procedures, Proceedings of Greener Aviation: Clean Sky breakthroughs and worldwide status, Brussels, Belgium, 2014.

[17] L. Trainelli, M. Lovera, A. Rolando, E. Zappa, M. Gennaretti, P. Cordisco, R. Grassetti, and M. Redaelli, Project MANOEUVRES – Towards real-time noise monitoring and enhanced rotorcraft handling based on rotor state measurements, 41st European Rotorcraft Forum ERF2015, Munich, Germany, 2015.

[18] R.W. Prouty. *Helicopter Performance, Stability and Control*. Robert E. Krieger Publishing Company, 1990.

[19] C.L. Bottasso, and C.E.D. Riboldi, Estimation of wind misalignment and vertical shear from blade loads, *Renewable Energy*, Vol. 26, 2014, pp. 293–302.

[20] D. Leonello, Project RSim Model Equations (RSim Release 2.0), internal report, AWParc, December 2011.

[21] D. Leonello, Project RSim Design Document (RSim Release 2.0), internal report, AWParc, February 2012.

[22] G. Padfield. *Helicopter Flight Dynamics.* Blackwell Science, 1996.